SCIENCE CHINA
Technological Sciences

•Article•

April 2019 Vol.62 No.4: 635–648
https://doi.org/10.1007/s11431-017-9220-8

Seismic performance assessment of high CFRDs based on fragility analysis

PANG Rui[1], XU Bin[1,2*], ZOU DeGao[1,2] & KONG XianJing[1,2]

[1] *School of Hydraulic Engineering, Faculty of Infrastructure Engineering, Dalian University of Technology, Dalian 116024, China;*
[2] *State Key Laboratory of Coastal and Offshore Engineering, Dalian University of Technology, Dalian 116024, China*

Received October 25, 2017; accepted February 26, 2018; published online September 7, 2018

Due to a large number of high concrete face rockfill dams (CFRDs) being constructed, the seismic safety is crucially important and seismic performance assessment must be performed for such dams. Fragility analysis is a method of great vitality for seismic performance assessment; it can intuitively forecast the structural effects of different ground motion intensities and provide an effective path for structure safety assessment. However, this method is rarely applied in the field of high earth dam risk analysis. This paper introduces fragility analysis into the field of high CFRD safety assessment and establishes seismic performance assessment methods. PGA, S_a (T_1, 5%), PGV and PGD are exploited as the earthquake intensity measure (IMs). Relative settlement ratio of dam crest, cumulative sliding displacement of dam slope stability and a new face-slab destroying index (based on DCR and COD) are regarded as the dam damage measures (DMs). The dividing standards of failure grades of high CFRDs are suggested based on each DM. Fragility function is estimated according to incremental dynamic analysis (IDA) and multiple stripes analysis (MSA) methods respectively from a large number of finite element calculations of a certain CFRD, and seismic fragility curves are determined for each DM. Finally, this study analyzes the failure probabilities of the dam under different earthquake intensities and can provide references and bases for the seismic performance design and safety risk assessment of high CFRDs.

high CFRDs, seismic performance, fragility analysis, failure grades, IDA, MSA

Citation: Pang R, Xu B, Zou D G, et al. Seismic performance assessment of high CFRDs based on fragility analysis. Sci China Tech Sci, 2019, 62: 635–648, https://doi.org/10.1007/s11431-017-9220-8

1 Introduction

Concrete face rockfill dams (CFRDs) are advantageous in terms of their short construction period, low investment cost, ease of construction, reliability and wide adaptability; due to these advantages, CFRDs have become the first choice for dam engineering [1]. With the growing demand for water resources and hydropower from the social economy, as well as the progress of and developments in damming technology, the height of CFRDs is continually increasing, with many dams being more than 200 m high and even reaching 300 m [2], e.g., Shuibuya dam (233 m), Jiangpinghe dam (219 m), and Houziyan dam (219.5 m) in China. Many of these dams are located in areas where there are a number of large-scale, high-intensity active faults. Once damaged by strong earthquakes, CFRDs may be destroyed or even collapse; thus, the safety of people and property will be threatened, and serious environmental problems may arise [3]. Consequently, the seismic safety and earthquake disaster risk of these high dams are key problems that must be considered. There are no cases in which 200 m or higher CFRDs have suffered from serious seismic hazard to date; therefore, it is critical to perform seismic performance assessments for CFRDs.

Seismic fragility analysis is an important and effective method for assessing seismic performance; it can forecast the probability of structural effects under different ground mo-

* Corresponding author (email: xubin@dlut.edu.cn)

tion intensities and provide a scientific basis for reasonable safety evaluation and decision making [4]. The method has been widely used to estimate the structural responses and analyze the stability of structures exposed to the action of different seismic intensities, e.g., architectural structures, bridge structures, and other types of life-line systems engineering. In recent years, some scholars have attempted to introduce this method into the preliminary seismic safety assessment of concrete dams; for example, Tekie and Ellingwood [5,6] obtained the fragility curves of dam body cracking, dam foundation slipping and dam toe for the Bluestone Gravity Dam by analysis of static and dynamic loads through LHS. Lin and Adams [7] presented a set of empirical seismic fragility curves for concrete dams located in eastern and western Canada with a mean DPM. Zhong et al. [8] considered both the uncertainties in ground motion records and concrete material using the MCS of a 296 m high arch dam, and the fragility curves were obtained through fitting the data points using the log-normalized CDF. Abdelhamid et al. [9] considered the aleatory and epistemic uncertainties simultaneously and derived the seismic fragility curves of an old gravity dam by adapting the methodology proposed by Tekie. Kadkhodayan et al. [10] performed a nonlinear analysis with the IDA for a 203 m high arch dam using nine three-component ground motion records and three potential intensity measures (IMs). Morales-Torres et al. [11] proposed a comprehensive procedure for the fragility analysis of the sliding failure of concrete dams, integrating natural and epistemic uncertainties. Ghanaat et al. [12] developed a set of fragility curves for different concrete dams using an approach that was fundamentally similar to the one proposed by Tekie. Hariri-Ardebili et al. developed modern fragility curves/surfaces for concrete dams with the MSA [13], CLA [14], IDA [15], and ETA [16]. Ansari and Agarwal [17] used an IDA approach for the structural analysis of a 122 m high gravity dam and derived fragility curves based on the ground motion IM and crest displacement EDP. These studies achieved a preliminary assessment of concrete dam safety and demonstrated that the seismic fragility analysis method was suitable for large water and hydropower engineering.

Currently, there are few fragility analyses for earth and rockfill dams, particularly high CFRDs. In addition to the increased calculation time, there are other reasons for the lack of analyses. First, the earthquake destruction patterns of earth and rockfill dams are varied, including seismic deformation, the destruction of the face-slab and slope failure. Second, the dam failure grades and standards are not mature or accepted. Third, the dam damage measures (DMs) corresponding to some assessment indices are unreasonable and cannot always effectively reflect the changing characteristics or influences under the action of earthquakes.

Due to the construction of a large number of high CFRDs, it is necessary to evaluate the seismic performance using a specific method, which can be achieved using a fragility analysis. Deformation, stability and anti-seepage structure safety are the main aspects that should be considered when evaluating the seismic safety of high CFRDs; therefore, it is more reasonable to investigate the seismic performance while considering these three aspects simultaneously. Generally, the relative settlement ratio of a dam crest [18,19], the cumulative sliding displacement of the dam slope stability [20] and the face-slab stress [21] are used as the dam DMs and correspond to the three performance assessment indices. However, with the construction of CFRDs in areas of strong earthquakes, the stress-based control standards are unable to meet the engineering requirements; the stress amplitude for exceeding tensile strength and the cumulative stress duration of the concrete have a large effect on face-slab safety. Therefore, a new face-slab destroying index that simultaneously considers the stress amplitude of exceeding tensile strength (called the demand-capacity ratio, DCR) and the cumulative overstress duration (COD) are the DMs relative to anti-seepage structure safety that are used in this study, which are based on a time history analysis of the linear elasticity of face-slab concrete. The three DMs used to perform the seismic fragility analysis will be introduced in Section 3.2. In addition, dividing standards of dam failure grades are also preliminarily suggested based on these three DMs for the fragility analysis and the basis is analyzed in Section 5.4.

In this paper, a fragility analysis is applied to perform a seismic performance assessment for high CFRDs based on three seismic performance assessment indices (deformation, stability and anti-seepage structure safety) using the IDA and MSA methods. Peak ground acceleration (PGA), spectral acceleration at structure's first mode period (S_a (T_1, 5%)) at 5% damping, peak ground velocity (PGV) and peak ground displacement (PGD) are selected as the earthquake IMs considering the uncertainty of earthquake ground motion inputs, and perform a brief comparison of their applicability. The relative settlement ratio of the dam crest, the cumulative sliding displacement of the dam slope stability and a new face-slab destroying index (based on the DCR and COD) are regarded as the dam DMs. Three failure grades are suggested as the standards of the dam; then, the fragility curves and probabilities of every failure grade based on the different performance indices are achieved through the seismic response analysis and fragility analysis of a certain high CFRD.

2 Fragility analysis method

Seismic fragility is a parametric analysis method that is based on a nonlinear dynamic time history analysis. There

are a number of procedures for carrying out a nonlinear dynamic analysis to collect data for estimating a fragility function. One common approach is the IDA, where a set of ground motions is repeatedly scaled to find the IM levels at which each ground motion causes collapse [22,23]. Another common approach is the MSA, where the analysis is performed at a specified set of IM levels, each of which has a unique ground motion set [24]. Finally, curves are established using these two methods where the IM is regarded as the horizontal axis and the probability of the structural response exceeding a certain limit state is regarded as the vertical axis. In general, according to related research [25,26], the fragility function is assumed to be a lognormal cumulative distribution function of double parameters defined as follows:

$$P_R(C|\mathrm{IM}=X)=\Phi\left[\frac{\ln(X/\theta)}{\sigma}\right], \tag{1}$$

where $P_R(C \mid \mathrm{IM}=X)$ is the probability of a certain performance level of the earthquake intensity IM=X; $\Phi()$ is the standard normal cumulative distribution function; θ is the logarithmic median and σ is the standard deviation of lnIM, where the earthquake IM reaches a certain performance level. Finally, a normal distribution function that regards the IM as the independent variable is established, and fragility curves are drawn. θ and σ can be estimated depending on the IDA or MSA. In this study, the fragility analysis based on relative settlement ratio of the dam crest and the cumulative sliding displacement of the dam slope stability is performed by IDA, however fragility analysis based on face-slab destroying index is carried out by MSA.

2.1 Incremental dynamic analysis

Incremental dynamic analysis (IDA) approach involves performing nonlinear analyses of a prototype structural system using a suite of ground motion records, with each scaled to several IM levels designed to force the structure to final global dynamic instability (severe failure). From the IDA curves, limit states can be defined and the probability of exceeding a specified limit state for a given IM (e.g., PGA, PGV, etc.) can be determined. The fragility function parameters can be estimated from these data by the logarithms of each ground motion's IM value associated with the onset of the limit state and computing their mean and standard deviation.

$$\ln\hat{\theta}=\frac{1}{n}\sum_{i=1}^{n}\ln\mathrm{IM}_i, \tag{2}$$

$$\hat{\sigma}=\sqrt{\frac{1}{n-1}\sum_{i=1}^{n}(\ln(\mathrm{IM}_i/\hat{\theta}))^2}, \tag{3}$$

where n is the number of ground motions considered, IM_i is the IM value associated with the onset of collapse for the ith ground motion, and $\ln\theta$ and σ are the mean and standard deviation of the normal distribution representing the lnIM values, respectively.

2.2 Multiple stripes analysis

Multiple stripes analysis (MSA) is an approach that adjusts the IMs to different intensity levels and conducts structural analysis at a discrete set of IM levels, ultimately yielding the number of IMs whose DMs exceed a certain limit state. This method is effective for multiple destroying indices that are simultaneously considered to be a structural DM, e.g., the face-slab destroying index using the DCR and COD. The fragility function parameters θ and σ can be determined with the maximum likelihood method; it is equivalent and numerically easier to maximize the logarithm of the likelihood function [24].

$$\begin{pmatrix}\hat{\theta}\\ \hat{\sigma}\end{pmatrix}=\arg\max\sum_{i=1}^{m}\left\{\ln\binom{n_i}{z_i}+z_i\ln\Phi\left(\frac{\ln(x_i/\theta)}{\sigma}\right)+(n_i-z_i)\ln\left[1-\Phi\left(\frac{\ln(x_i/\theta)}{\sigma}\right)\right]\right\}, \tag{4}$$

where z_i is the number of observed failures exceeding a certain limit state in n_i ground motions and m is the number of IM levels.

3 Ground motion records and performance parameters

3.1 Selection of ground motion records

According to previous studies [27], 10–20 ground motion records have completely met the requirements needed to estimate the seismic demand of structures. In this paper, the ground motion inputs adopted an artificial seismic record and 14 actual seismic records. The response spectrum based on the site conditions of a high earth rockfill dam in China is chosen to be the target spectrum. As described in eq. (1), $\beta(T)$ is the magnification response spectrum of ground motion acceleration, and T_1=0.12 s, T_2=0.34 s, $\beta_{\max}$=2.2, and γ=1.0. One seismic wave is artificially generated based on the target response spectrum. Then, 14 actual ground motion records that correspond well to the target response spectra are selected in PEER (http://ngawest2.berkeley.edu/, 24 May 2016). The magnitude of these waves is 6.0–7.0, and the PGA>0.2 g; information about these 15 ground motion records is provided in Table 1. The acceleration time histories of the artificial seismic wave are shown in Figure 1, and the acceleration response spectra of the 15 earthquake waves are shown in Figure 2 (the bold continuous line is the average response spectrum, and the dashed line is the target response spectrum). Obviously, the average response spectrum is well

Table 1 The earthquake records used in the fragility analysis

No.	Earthquake name	Recording stations	Magnitude	Rjb (km)	PGA (g)	Year
1	Imperial Valley-06	El Centro Array #11	6.53	12.56	0.367	1979
2	Imperial Valley-06	Calexico Fire Station	6.53	10.45	0.277	1979
3	Imperial Valley-06	El Centro Array #3	6.53	10.79	0.267	1979
4	Mammoth Lakes-01	Long Valley Dam	6.06	12.56	0.430	1980
5	Loma Prieta	Gilroy Array #2	6.93	10.38	0.370	1989
6	Loma Prieta	San Jose-Santa Teresa Hills	6.93	14.18	0.276	1989
7	Northridge-01	LA 00	6.69	9.87	0.263	1994
8	Northridge-01	Sun Valley-Roscoe Blvd	6.69	5.59	0.277	1994
9	Northwest China-03	Jiashi	6.1	9.98	0.300	1997
10	Tottori Japan	SMN001	6.61	14.42	0.236	2000
11	San Simeon CA	Templeton-1-story Hospital	6.52	5.07	0.435	2003
12	Niigata Japan	NIGH12	6.63	9.93	0.417	2004
13	Iwate Japan	AKT023	6.9	11.68	0.368	2008
14	Iwate Japan	Kurihara City	6.9	12.83	0.422	2008
15	Artificial seismic wave					

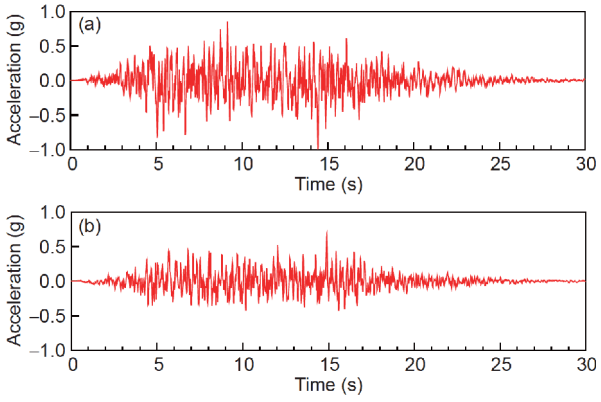

Figure 1 (Color online) Time histories of input ground motion. (a) Transverse direction; (b) vertical direction.

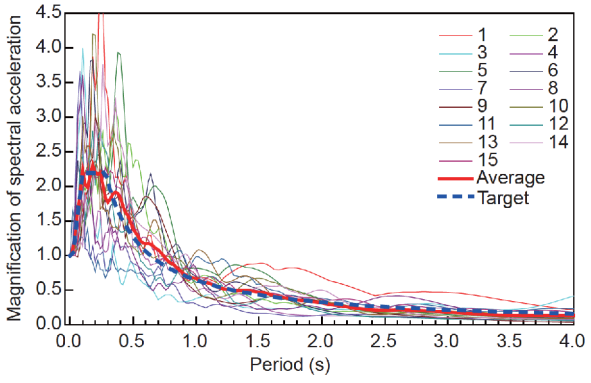

Figure 2 (Color online) The earthquake acceleration response spectrum curves.

matched with the target response spectrum, which indicates that the selected seismic records are reasonable.

$$\beta(T)=\begin{cases}1,\ T\le 0.04\ \text{s},\\ 1+(\beta_{\max}-1)\dfrac{T-0.04}{T_1-0.04},\ 0.04\ \text{s}<T\le T_1,\\ \beta_{\max},\ T_1<T\le T_2,\\ \beta_{\max}\left(\dfrac{T_2}{T}\right)^{\gamma},\ T_2<T\le 6\ \text{s}.\end{cases}\tag{5}$$

3.2 Selection of the dam damage measures

In this paper, three dam DMs (the relative settlement ratio of the dam crest, the cumulative sliding displacement of the dam slope stability and the face-slab destroying index based on the DCR and COD) are selected to perform the seismic fragility analysis with different failure grades. The dam DMs are briefly described below.

(1) Relative settlement ratio of the dam crest: Ratio of the permanent deformation of the dam crest to the dam height after the earthquake [18,19].

(2) Cumulative sliding displacement of the dam slope: The sliding displacement to which the most dangerous slipping arc corresponds while conducting a finite element stability analysis of the dynamic time history of the dam [28,29].

(3) Face-slab destroying index: the demand capacity ratio (DCR) and cumulative overstress duration of the face slab, DCR=σ_t/f_s (σ_t is the calculated tensile stress, and f_s is the tensile strength), cumulative overstress duration (cumulative time that the calculated tensile stress exceeds the tensile strength), as discussed in detail in ref. [30].

4 Constitutive model

The properties of rockfills under monotonic and cyclic loading, such as particle breakage [31–34], critical state [34–

36], and dilatancy [37,38], are complicated. Many researchers have emphasized on this issue and some elasto-plastic models [21,33] are proposed recently. However, the parameters for these models are difficult to determine and less engineering experience can be given. In this paper, the Duncan-Chang model [39] described in Section 4.1 was used to simulate the behavior during construction and impounding process. In Section 4.2, the model improved by Shen and Xu [40] based on the Hardin and Drnevich [41] model was introduced and used in the dynamic analysis. Because of the limitation of the H-D model, the residual deformation could not be obtained directly, so the method of strain potential was used to solve this problem. In Section 4.3, the modified Shen Zhu-jiang residual deformation model [42] was introduced and this model was used to determine the equivalent nodal force for calculating the residual seismic deformation. The three models for rockfilss were introduced as following.

4.1 Duncan-Chang model for rockfill

Duncan and Chang [39] proposed a hyperbolic model based on the stress and strain results of triaxial experiments. At present, the model is widely used in pre-seismic stress and strain characteristics analyses of earth dams, and the numerical results are consistent with the in situ measurements [43,44]. The model accounts for the loading/unloading stress path and the hyperbolic dependency of the elasticity modulus on the current stress state. The parameters involved can be readily determined from well-studied triaxial data despite the dilatancy and the plasticity not being well-expressed. In this study, the Duncan-Chang model was employed to describe the behavior of the dam materials.

4.2 Shen Zhu-jiang dynamic model for rockfill

The model employed in the equivalent-linear analysis is simple, and previous studies have accumulated a large amount of experimental data and engineering experience in the determination and application of parameters. The Shen Zhu-jiang dynamic model is an equivalent linear viscoelastic model that was proposed by Shen and Xu [40] based on the Hardin and Drnevich [41] model and has been used extensively in the study of embankment dams to establish the seismic stress-strain state.

The relationship between the equivalent dynamic shear modulus G_{eq} and dynamic shear strain γ_d can be described as follows:

$$G_{eg} = \frac{k_2}{1+k_1\gamma_d} \cdot p_a \cdot \left(\frac{p}{p_a}\right)^n. \tag{6}$$

Then, the relationship between the equivalent damping ratio λ_{eq} and dynamic shear strain γ_d can be obtained as follows:

$$\lambda_{eq} = \lambda_{max} \cdot \frac{k_1 \cdot \bar{\gamma}_d}{1+k_1 \cdot \bar{\gamma}_d}, \tag{7}$$

where p is average effective stress, p_a is the technical atmosphere pressure, and k_1, k_2 and n are experimental parameters.

4.3 Modified Shen Zhu-jiang residual deformation model

The equivalent-linear analysis model can calculate the time history curves of the dynamic stress and strain during earthquakes; however, it is not suitable for calculating the permanent deformation after the earthquake. An equivalent nodal force method is necessary to consider the seismic force. There are many models based on the equivalent nodal force method that are widely used to calculate the residual deformation, including the Taniguchi model, modified Taniguchi model, IWHR model, Shen Zhu-jiang model and modified Shen Zhu-jiang model.

Based on dynamic triaxial experiments of drainage conditions, Shen and Xu [40] obtained the relationship between residual volumetric strain ε_{vr} and residual shear strain γ_r along with changes in the stress state with vibration time as follows:

$$\varepsilon_{vr} = c_{vr}\log(1+N), \tag{8}$$

$$\gamma_r = c_{dr}\log(1+N), \tag{9}$$

and

$$c_{vr} = c_1\gamma_d^{c_2}\exp(-c_3S_1^2), \tag{10}$$

$$c_{dr} = c_4\gamma_d^{c_5}S_1^2. \tag{11}$$

Based on the logarithmic coordinates treating the natural constant e as a base, the increment forms of the residual volumetric strain and residual shear strain in eqs. (10) and (11) are

$$\Delta\varepsilon_{vr} = c_1\gamma_d^{c_2}\exp(-c_3S_1^2)\frac{\Delta N}{1+N}, \tag{12}$$

$$\Delta\gamma_r = c_4\gamma_d^{c_5}S_1^2\frac{\Delta N}{1+N}, \tag{13}$$

where $\Delta\varepsilon_{vr}$ is the residual volumetric strain increment, $\Delta\gamma_r$ is the residual shear strain increment, γ_d is the dynamic strain amplitude, S_1 is the stress level, N and ΔN are the total vibration frequency and time increment, respectively, and c_1, c_2, c_3, c_4, and c_5 are experimental parameters.

The formulas above are developed from sandy soil experiments. For rockfill, Zou et al. [42] improved the calculation model through a large number of large-scale cycle triaxial experiments. The modified expression is

$$c_{dr} = c_4\gamma_d^{c_5}S_1^n, \tag{14}$$

where n is the stress level index and is typically 0.9–1.0.

4.4 Dynamic analysis method for sliding

As shown in Figure 3, the safety factor is the ratio of the maximum shear strength that can be provided by the soil on the potential sliding surface to the actual shear stress produced by the external loading on the potential sliding surface. A stability calculation will be performed according to the superimposed results of the static and dynamic stress based on Newmark method [28,29,45]. The safety factor is as follows:

$$F_s = \frac{\sum_{i=1}^{n}(c_i + \sigma_{ni}\mathrm{tg}\phi_i)l_i}{\sum_{i=1}^{n}\tau_i l_i}, \tag{15}$$

$$\sigma_n = \frac{\sigma_x + \sigma_y}{2} - \frac{\sigma_x - \sigma_y}{2}\cos 2\alpha - \tau_{xy}\sin 2\alpha, \tag{16}$$

$$\tau = \frac{\sigma_x - \sigma_y}{2}\sin 2\alpha - \tau_{xy}\cos 2\alpha, \tag{17}$$

where c_i and ϕ_i are the cohesion and friction angle, respectively; l_i is the length of element i, which crosses the slip circle; σ_{ni} and τ_i are the normal stress and tangential stress of element i, respectively; $\sigma_x = \left(\sigma_x{}^s + \sigma_x{}^d\right)$; $\sigma_y = \left(\sigma_y{}^s + \sigma_y{}^d\right)$; $\tau_{xy} = \left(\tau_{xy}{}^s + \tau_{xy}{}^d\right)$; $\sigma_x{}^s$ is the horizontal static stress; $\sigma_x{}^d$ is the horizontal dynamic stress; $\sigma_y{}^s$ is the vertical static stress; $\sigma_y{}^d$ is the vertical dynamic stress; $\tau_{xy}{}^s$ is the static shear stress; and $\tau_{xy}{}^d$ is the dynamic shear stress. The angular acceleration after the loss of stability is

$$\ddot{\theta}(t) = \frac{M}{I}, \tag{18}$$

$$M = \left(\sum_{i=1}^{n}\tau_{ni}l_i - \sum_{i=1}^{n}(c_i + \sigma_{ni}\tan\phi_i)l_i\right)R, \tag{19}$$

where I is the inertia; M is the rotating moment of the sliding block; and R is the slip radius of the circle.

Instantaneous sliding occurs throughout the process, and the cumulative slide displacement is

$$D_{ik} = R^k\theta_1{}^k = R^k\iint\ddot{\theta}^k\mathrm{d}t, \tag{20}$$

$$D_k = \sum_{i=1}^{n}D_{ik}. \tag{21}$$

The maximum sliding displacement is

$$D_{\max} = \mathrm{Max}(D^1, D^2, ..., D^k, ..., D^m). \tag{22}$$

4.5 Interfaces and peripheral joints

The contact surface between the cushion and the face slab adopts Goodman zero-thickness elements [46]. This hyperbolic model for contact elements is widely used to simulate the CFRDs' contact between the cushion and the face slab [47]. The parameters are precisely calibrated based on corresponding experimental results [48]. The formulas and parameters of the interface elements are described in ref. [47].

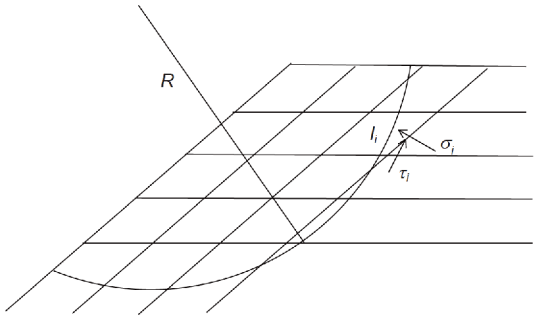

Figure 3 Schematic diagram of the safety factor calculation.

According to ref. [48], the parameters of the joints are assumed to be constant, with a compressive stiffness of 25000 MPa m^{-1} and a shear stiffness of 1 MPa m^{-1} in the shear direction. The peripheral joints are established between the face slabs and plinth.

5 Finite element analysis

The calculation procedure adopted is the geotechnical engineering software GEODYNA (Geotechnical Dynamic Nonlinear Analysis), which was independently developed by the authors' team [49]. The distribution characteristics and changing rules of the performance parameters using different earthquake intensities from different seismic records are analyzed in detail by performing 2D nonlinear finite element numerical calculations for a 242-m-high CFRD. The dam fragilities at different earthquake intensities are obtained. The finite element model, constitutive models and calculating parameters are introduced in the following sections.

5.1 Finite element model

The 2D finite element model of the CFRD has a maximum height of 242 m and a top width of 25 m. The upstream dam slope is 1:1.5, and the berm height is 188 m. The downstream dam slope above the berm is 1:1.7, whereas the dam slope under the berm is 1:1.4. There are two-layer transition zones with every layer 4 m wide and cushion zones with a width of 4 m following the face slab. The dam is filled with 102 layers, and the face slabs are poured in three stages (122, 192 and 242 m). Impounding begins when the face slabs have been poured, and the height of the impounded water is 220 m. The finite element mesh of the CFRD is shown in Figure 4. In the dynamic calculations, the hydrodynamic pressure of the face slab is simulated with the added mass method [50]. The simplified Westergaard formula used and the added mass intensity on the face-slabs can be expressed

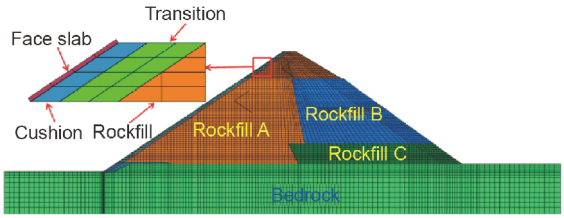

Figure 4 (Color online) Finite element mesh of CFRD.

as

$$m_{\omega i} = \frac{\theta}{90}\frac{7}{8}\rho\sqrt{H_0 y_i}\,A_i, \tag{23}$$

where ρ is the water density, θ is angle of the upstream slope, H_0 is the depth from the position of node i to the bottom of reservoir, y_i is the depth from water surface to position of node i, and A_i is the control area of node i. The added mass under the water level during earthquake can be computed by integrating $m_{\omega i}$ on the surface of the face-slabs, which yields 66 added mass elements totally.

5.2 Constitutive models and material parameters for calculations

The static calculations of rockfill are simulated by the Duncan *E-B* nonlinear elastic constitutive model, and the dynamic calculations are simulated by the Shen Zhu-jiang model. The permanent deformation calculations are simulated by the modified Shen Zhu-jiang residual deformation model. The dynamic stability calculations adopt the dynamic analysis method for sliding. The rockfill parameters of every model are shown in Tables 2–4. The bedrock is based on a linear elastic model, with the following parameters: density ρ =2600 kg m^{-3}, elastic modulus E=20 GPa and Poisson's ratio v=0.25.

A linear elastic model, which is sufficient to represent the influence of the hydrodynamic pressure on a slab, is chosen to simulate the behavior of the concrete face slabs. In accordance with the typical design specifications for an extremely high CFRD, the face slabs are assumed to consist of C30 concrete, which has the following properties: a density of ρ=2.40 g cm^{-3}, a modulus of elasticity of E=30 GPa and a Poisson's ratio of v=0.167. The compressive strength of the face slab is 27.6 MPa, and the tensile strength under static and seismic dynamic loads is calculated using the formulas recommended by Raphael [51]. The static tensile strength is 3 MPa.

5.3 Ground motion input

The input ground motion is achieved through a viscoelastic boundary and an equivalent load. The equivalent load can be

Table 2 Parameters for Duncan *E-B* model

Materials	ρ (kg m^{-3})	K	n	R_f	K_b	m	φ_0 (°)	$\Delta\varphi$ (°)
Rockfill A	2214	1350	0.28	0.80	780	0.18	55.5	11.3
Rockfill B	2214	1000	0.26	0.79	700	0.16	53.0	11.0
Rockfill C	2214	1300	0.31	0.79	800	0.12	55.0	12.2
Transition	2222	1250	0.31	0.78	500	0.16	53.5	10.7
Cushion	2258	1200	0.30	0.75	680	0.15	54.4	10.6

Table 3 Parameters for Shen Zhu-jiang dynamic model

Materials	k_1	k_2	n	λ_{max}
Rockfill A	32	2570	0.471	0.22
Rockfill B	48	3668	0.377	0.22
Rockfill C	65	5596	0.268	0.17
Transition	36	3383	0.413	0.20
Cushion	2258	1200	0.30	0.17

Table 4 Parameters for residual deformation calculations

Materials	c_1 (%)	c_2	c_3	c_4 (%)	c_5
Rockfill A	1.36	0.85	0.00	23.26	0.74
Rockfill B	3.46	1.03	0.00	31.46	0.83
Rockfill C	0.84	0.81	0.00	10.82	0.62
Transition	1.45	0.97	0.00	4.91	0.51
Cushion	1.45	0.97	0.00	4.91	0.51

calculated using the following equation [52]:

$$\mathbf{F}_b = \mathbf{R}_b^{ef} + \mathbf{C}_b\dot{\mathbf{u}}_b^{ef} + \mathbf{K}_b\mathbf{u}_b^{ef}, \tag{24}$$

where $\mathbf{u}_b^{ef}$, $\dot{\mathbf{u}}_b^{ef}$ and $\mathbf{R}_b^{ef}$ are the displacement vector, velocity vector and the corresponding force vector induced at the system boundary nodes by the free wave field, respectively, and $\mathbf{K}_b$ and $\mathbf{C}_b$ are the additional stiffness matrix and damping matrix of the boundary element caused by the viscoelastic artificial boundary, respectively. Viscoelastic boundary elements are added at the bottom and sides of the bedrock, and the equivalent load is applied to the internal nodes of boundary elements.

5.4 Proposal of dam failure grades

The failure grades are the different limit states of damage. In this study, a three-level failure grades for high CFRDs is proposed based on three indices permanent deformation, stability of the dam slope and face-slab seismic safety.

5.4.1 Seismic permanent deformation

Currently, the control standards for post-earthquake deformation of high CFRDs are suggested to be a relative settlement ratio of 0.6%–0.8% [18,19]. Swaisgood [53] surveyed 69 dams (including CFRDs, core wall rockfill dams, hydraulic fill dams and earth dams), regarded the relative settlement ratio of the dam crest as an index, and divided the earthquake destroying situation into four failure grades: healthy (<0.1%), minor (0.012%–0.5%), moderate (0.1%–1.0%) and severe (>0.5%).

In this study, the related safety assessment and grading standards mentioned above are used to establish three limit failure states with relative settlement ratios of 0.4%, 0.7%, and 1.0% for the dam crest, and suggest the corresponding three failure grades of minor, moderate and severe, respectively.

5.4.2 Stability of the dam slope

Several studies and specifications have focused on the safety of dam slope stability with cumulative sliding displacement. Switzerland [54] adopted two-level seismic design standards, with allowable deformations of 20 cm (shallow sliding) and 50 cm (deep sliding). Hyness and Franklin proposed a control standard of seismic sliding deformation of 1 m [20]. Tian et al. [55] considered a dam slope to have lost its balance when the cumulative slippage exceeded 1 m or 1% of the sliding length.

In this paper, three limit failure states with cumulative sliding displacement of 1 (barely sliding), 50, and 100 cm were selected corresponding to three failure grades of minor, moderate and severe, respectively.

5.4.3 Face-slab seismic safety

In the framework of linear elasticity, the control standards focus on the face-slab stress and joint displacement. Ghanaat [30] used the results of an elastic time-history analysis to obtain the ratio of the maximum tensile stress to tensile strength of concrete, called the demand-capacity ratio (DCR), and the cumulative time during which the maximum tensile stress exceeds tensile strength of concrete (DCR>1) in the process of the earthquake, called the cumulative overstress duration, and finally proposed the standards for failure grades for concrete dams.

This study, considering the face slab, uses the aforementioned assessment method to conduct a safety assessment and divide the failure grades based on changes in the face-slab stress. The recommended failure grades are as follows: (1) minor or no failure: the face-slab response is considered to be within the linear elastic range of behavior with little or no possibility of destruction if DCR≤1; (2) minor-moderate failure: the face-slab exhibits cracking, and the DCR and cumulative overstress duration are in the shaded part of Figure 5; (3) severe failure: DCR>2 or the cumulative overstress duration is beyond the shaded part; a nonlinear time-history analysis may be required in this situation.

6 Seismic fragility analysis

6.1 IDA and MSA results

In this study, four IMs are used for the IDA and MSA namely: PGA, S_a (T_1, 5%), PGV and PGD. In the IDA with the relative settlement ratio of the dam crest and the cumulative sliding displacement, amplitude modulation of the IMs (PGA, S_a (T_1, 5%), PGV, PGD) with equal intervals was performed until the failure of the different dam DMs reached the severe level (no failure to severe failure). The equal intervals of each ground motion corresponding to every IM are listed in Table 5. The different intensity discrete levels of the IMs based on the MSA with the face-slab destroying index

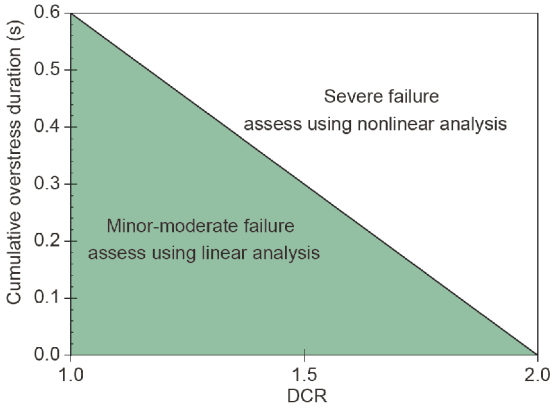

Figure 5 (Color online) Seismic performance and destroying evaluation standards of face-slab.

Table 5 Equal intervals of each ground motion corresponding to every IM

No.	Earthquake name	PGA (g)	S_a (T_1, 5%) (g)	PGV (m s^{-1})	PGD (m)
1	Imperial Valley-06	0.1	0.013	0.083	0.051
2	Imperial Valley-06	0.1	0.070	0.083	0.036
3	Imperial Valley-06	0.1	0.044	0.070	0.038
4	Mammoth Lakes-01	0.1	0.051	0.056	0.018
5	Loma Prieta	0.1	0.022	0.057	0.028
6	Loma Prieta	0.1	0.053	0.096	0.274
7	Northridge-01	0.1	0.027	0.034	0.036
8	Northridge-01	0.1	0.048	0.037	0.015
9	Northwest China-03	0.1	0.026	0.067	0.010
10	Tottori Japan	0.1	0.040	0.078	0.056
11	San Simeon CA	0.1	0.068	0.068	0.039
12	Niigata Japan	0.1	0.070	0.066	0.049
13	Iwate Japan	0.1	0.097	0.064	0.072
14	Iwate Japan	0.1	0.063	0.071	0.048
15	Artificial seismic wave	0.1	0.069	0.094	0.220

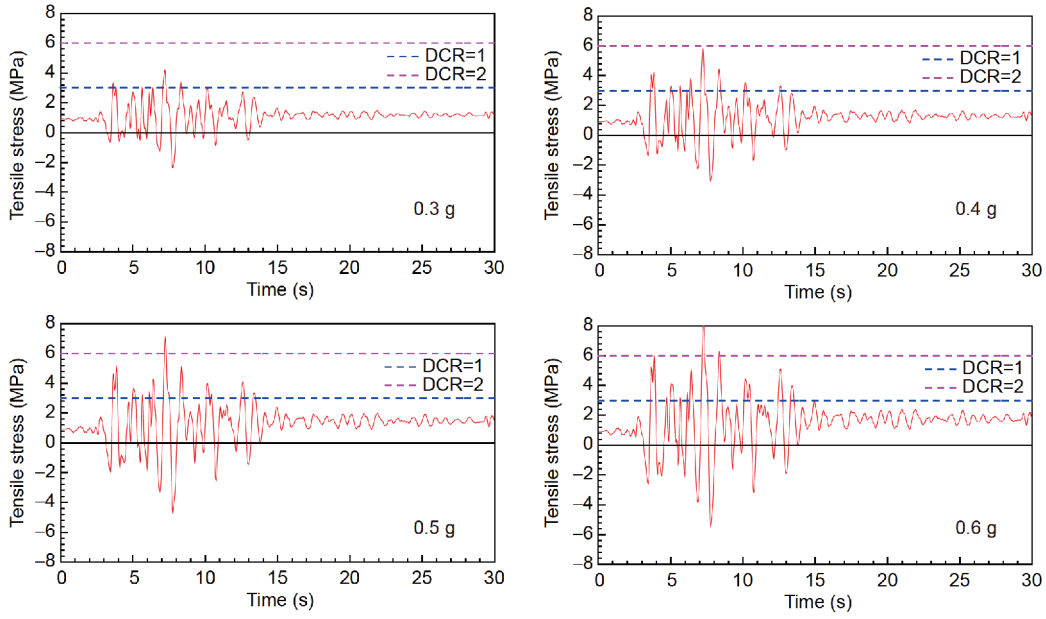

Figure 6 (Color online) Cumulative overstress duration for two DCRs using stress time histories in four PGA levels (No.12 waves).

are as follows: PGA (0.1, 0.2, …, 1.1, 1.2 g), S_a (T_1, 5%) (0.05, 0.1, …, 0.45, 0.5 g), PGV (0.05, 0.1, …, 0.55, 0.6 m s^{-1}), and PGD (0.05, 0.1, …, 0.45, 0.5 m). The peak vertical acceleration is 2/3 of the peak acceleration along the river. Many finite element calculations were performed to obtain the changing characteristics of the permanent deformation, cumulative sliding displacement and maximum tensile stress time histories of the face slab; Figure 6 illustrates the duration of tensile stress at four levels (PGA=0.3, 0.4, 0.5, and 0.6 g) during the seismic excitation at 1.0≤DCR≤2.0 and Figure 7 shows the performance curves (DCR versus COD) of the face-slab (represented by the No.12 wave). Then, the IDA curves of the IM relative set-

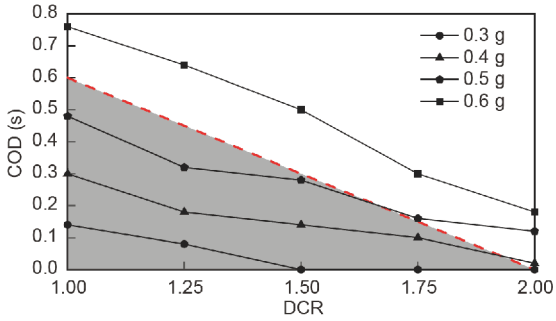

Figure 7 (Color online) Performance curves for the face-slab using linear elastic analysis (No.12 waves). DCR, demand capacity ratio; COD, cumulative overstress duration.

tlement ratio of the dam crest and IM cumulative sliding displacement are acquired, as shown in Figure 8, and the number of different failure grades of the different IM levels is listed in Table 6 based on the MSA. As shown in Figure 8 and Table 6, the uniformity of distribution using S_a (T_1, 5%) and PGA are better than that using PGV and PGD. Especially, in these curves where S_a (T_1, 5%) is selected as IM, there is strict consistency between various records. These results show that the dam's responses are essentially depend on the first-mode spectral acceleration of stream component,

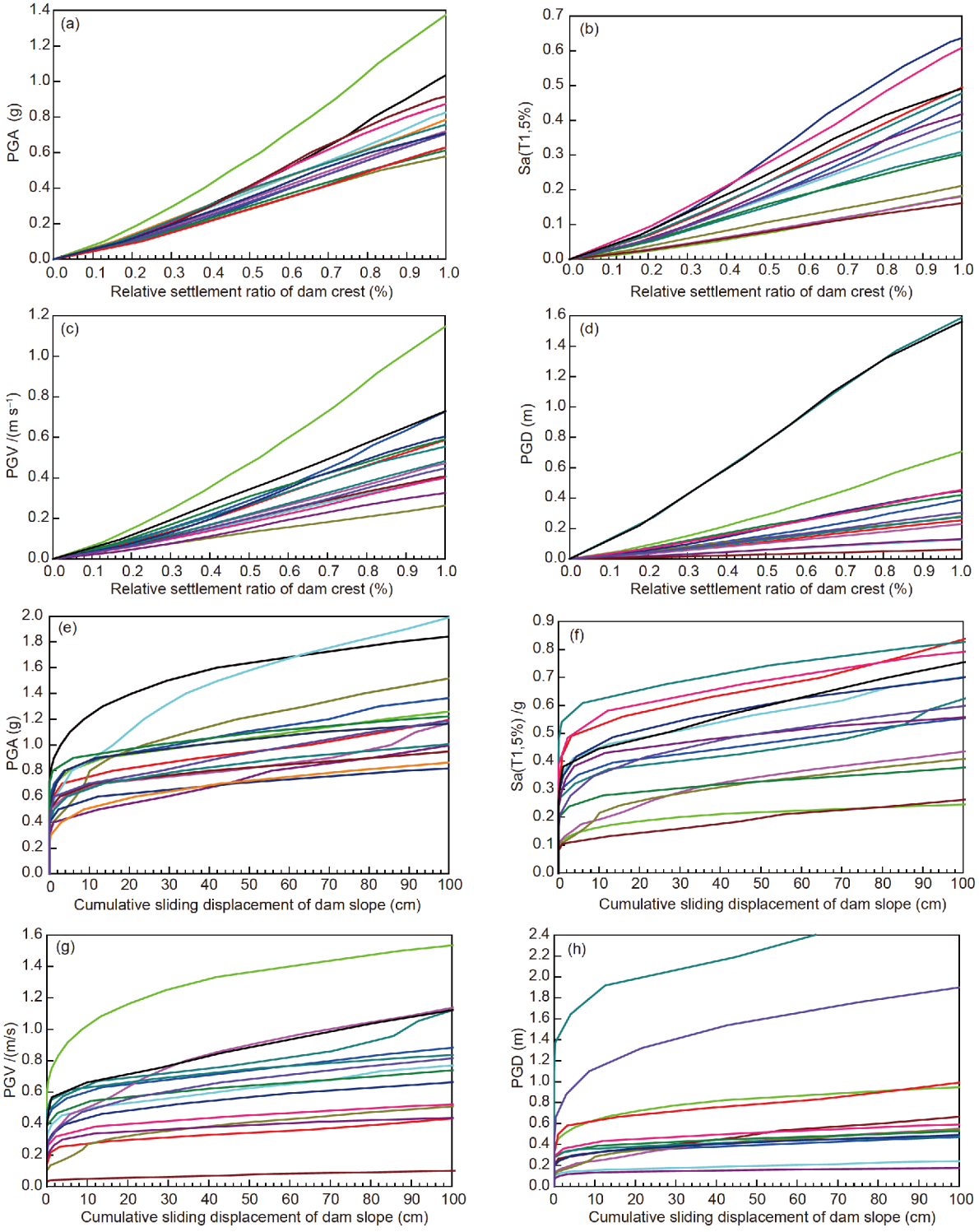

Figure 8 (Color online) IDA curves for different DMs. (a) Relative settlement ratio of dam crest with PGA; (b) relative settlement ratio of dam crest with S_a (T_1, 5%); (c) relative settlement ratio of dam crest with PGV; (d) relative settlement ratio of dam crest with PGD; (e) cumulative sliding displacement with PGA; (f) cumulative sliding displacement with S_a (T_1, 5%); (g) cumulative sliding displacement with PGV; (h) cumulative sliding displacement with S_a PGD.

Table 6 Number of different failure grades in different IMs levels based on MSA

PGA			S_a (T_1, 5%)			PGV			PGD		
Level (g)	Minor	Mederate	Level (g)	Minor	Mederate	Level (m s^{-1})	Minor	Mederate	level (m)	Minor	Mederate
0.1	0	0	0.05	0	0	0.05	0	0	0.05	1	0
0.2	0	0	0.1	2	0	0.1	0	0	0.1	3	2
0.3	4	0	0.15	7	1	0.15	0	0	0.15	6	3
0.4	10	1	0.2	7	3	0.2	5	0	0.2	11	4
0.5	13	4	0.25	13	5	0.25	8	2	0.25	12	5
0.6	14	8	0.3	15	5	0.3	12	2	0.3	13	9
0.7	15	11	0.35	15	10	0.35	13	4	0.35	13	10
0.8	15	11	0.4	15	12	0.4	13	6	0.4	13	12
0.9	15	11	0.45	15	15	0.45	14	10	0.45	13	12
1	15	13	0.5	15	15	0.5	15	12	0.5	13	12
1.1	15	14				0.55	15	13			
1.2	15	15				0.6	15	13			

and the responses to different earthquakes scaled to the same S_a (T_1, 5%) is predictable. The PGA is also relatively appropriate to be selected as the IM, however the PGV and PGD should be considered with discretion. Fragility curves are constructed using these response statistics in Figure 8 and Table 6 in terms of different selected IMs, PGA, S_a (T_1, 5%), PGV and PGD.

6.2 Fragility curves

We perform three-dimensional spline interpolations for every IDA curve for the relative settlement ratio of the dam crest and the cumulative sliding displacement of slope stability, and perform the MSA for the face-slab destroying index using two destroying indices (DCR and COD). The fragility curves corresponding to every failure grade of the three seismic performance assessment indices are obtained according to Section 2, as illustrated in Figure 9(a1)–(a3), and Table 7 show the probabilities for the representative IM levels. Seen from the Figure 9(a1)–(a3) and Table 7, deformation is easiest to happen, when PGA=0.4 g, minor failure has occurred completely (98.1%), and when PGA =0.6 g, the probability of moderate failure has reached to very big (73.8%). The face-slab safety also should be payed attention to, when PGA=0.4 g, the probability of minor failure has been very big (63.4%), and the probability of moderate failure is also big when PGA=0.6 g. However, the stability of dam slope is very high even under strong earthquake. Synthetically, the safety of this high CFRD is high considerably. The Figure 9(b)–(d) and Table 7 also support these points, and different failure probabilities can be seen based on other IMs. The probabilities of severe failure of all three indices reached to 50% at PGA=1.2 g, S_a (T_1, 5%) =0.5 g, PGV=0.6 m s^{-1} and PGD=0.6 m, which further indicate this dam safety is very high. The dam slope stability was high in a weak earthquake; however, a strong earthquake greatly affected the dam slope stability, and the failure probabilities changed rapidly.

With careful attention to these results (Figure 9; Table 7), it has been shown that choosing different IMs leads us to overestimate or low estimate the failure probability of the dams. The PGV and PGD fragility curves are a bit different from the PGA and S_a (T_1, 5%). Furthermore, the first vibration mode of the dam changes during seismic loading. Therefore, it seems the PGA to be more to form fragility curves for the considered high CFRDs. Moreover, the comparison should be done between the optimal spectral IM and the other spectral IMs that follow in the future study.

7 Conclusions

In this study, a seismic safety assessment on a high CFRD was conducted with the help of a fragility analysis. The main conclusions of the study are as follows.

(1) Fragility analysis was introduced into the seismic safety assessment field of high CFRDs, and a dam seismic performance evaluation method was developed based on permanent deformation, slope stability and face-slab safety. The method effectively considered the randomness of ground motion inputs and comprehensively assessed the seismic performance of dams. The probabilities of every seismic performance assessment index under different actions of an earthquake were obtained, and the standard or reference for dam seismic performance in strong earthquakes was provided. The results illustrate that this method has good applicability to seismic performance assessment.

(2) The relative settlement ratio of the dam crest, the cumulative sliding displacement of dam slope stability, and a new face-slab destroying index (DCR and COD) were sug-

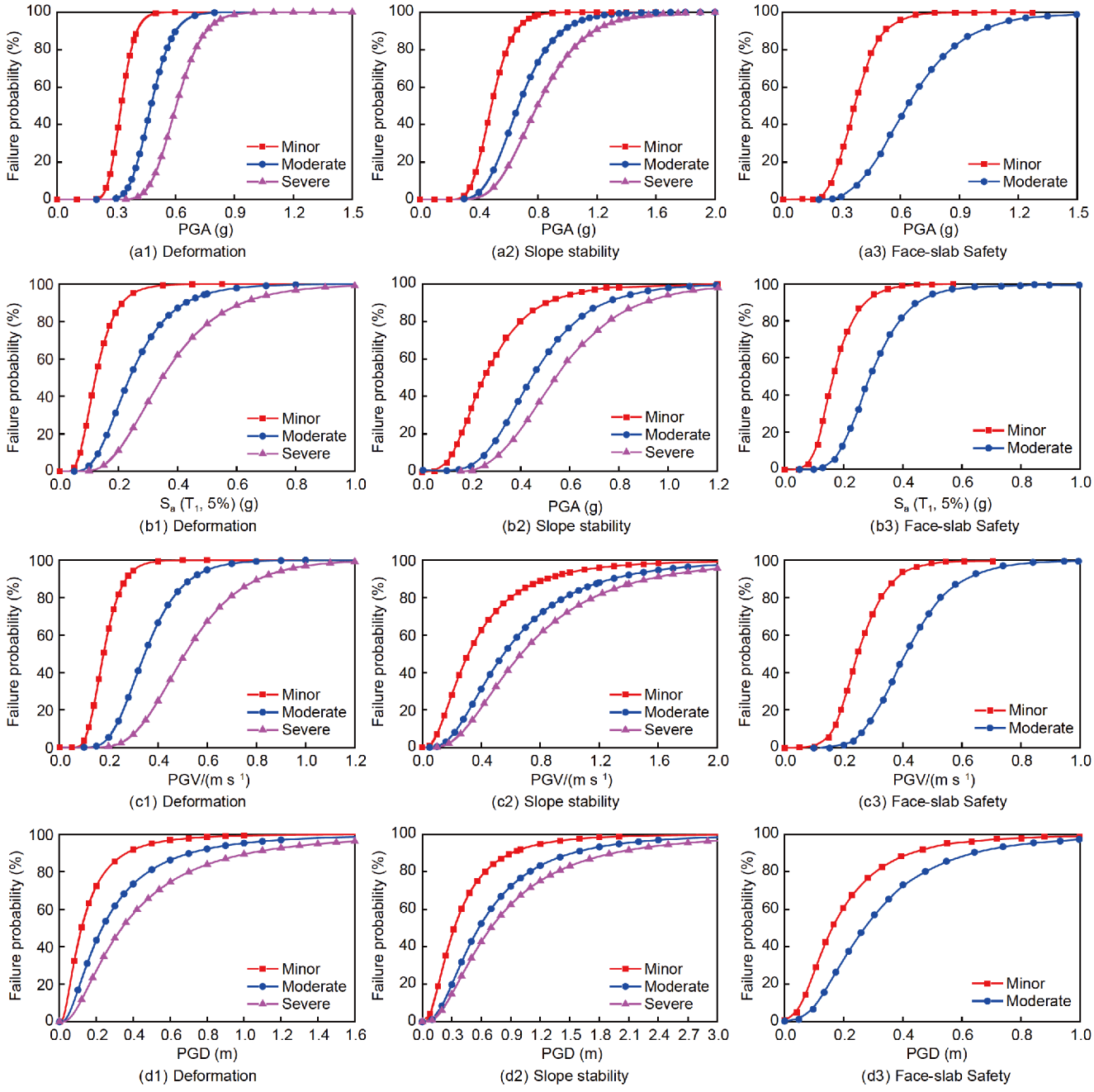

Figure 9 (Color online) Seismic fragility curves for all different IMs of every performance index.

gested as dam DMs and the PGA, S_a (T_1, 5%), PGV and PGD were used as the earthquake IMs. In addition, the selective basis was analyzed briefly. These measures provided appropriate performance indices of failure and seismic intensity characteristics for fragility analysis.

(3) In this paper, the limit states of failure grades were suggested, which applied to different performance indices of high CFRDs. The seismic performance levels of three grades (minor failure, moderate failure and severe failure) were determined, and the dividing criteria were discussed.

(4) Fragility curves and failure probabilities corresponding to the performance indices of different failure grades through a dam fragility analysis based on the IDA and MSA were presented, which provided a reference for decisions regarding the seismic design, reinforcement and maintenance of high CFRDs. However, the seismic fragility analysis is in the initial stages in terms of its application to earth and rockfill dams and requires further research.

(5) Fragility analysis of the high CFRD against PGA, S_a (T_1, 5%), PGV and PGD showed that the safety of this CFRD is very high.

(6) PGA and S_a (T_1, 5%) are two suitable IMs for a fragility

Table 7 Failure probabilities of every dam performance index based on different IMs

IMs	Performance index	Permanent deformation			Slope stability			Face-slab safety		
	Failure grade	Minor	Moderate	Severe	Minor	Moderate	Severe	Minor	Moderate	Severe
PGA	0.2 g	4.90%	0	0	0	0	0	1.50%	0	Assess using nonlinear analysis
	0.4 g	98.10%	8.90%	0.20%	11.60%	0	0	63.40%	9.90%	
	0.6 g	100%	73.80%	12.60%	61.90%	3.40%	0.60%	96.50%	44.40%	
	0.8 g	100%	98.00%	55.20%	91.40%	22.90%	7.70%	99.80%	75.00%	
	1.0 g	100%	100%	87.00%	98.60%	53.80%	27.20%	100%	90.40%	
	1.2 g	100%	100%	97.40%	100%	78.20%	52.60%	100%	96.60%	
S_a (T_1, 5%)	0.1 g	32.30%	2.90%	0.30%	4.70%	0	0	8.50%	0.10%	Assess using nonlinear analysis
	0.2 g	87.10%	35.30%	11.00%	33.70%	2.30%	0.60%	70.10%	14.20%	
	0.3 g	98.00%	69.50%	37.00%	62.30%	16.20%	6.90%	94.90%	54.80%	
	0.4 g	99.70%	87.20%	62.00%	79.90%	39.30%	22.30%	99.20%	83.30%	
	0.5 g	100%	94.80%	78.80%	89.30%	61.10%	42.00%	100%	98.50%	
	0.6 g	100%	97.90%	88.50%	94.20%	76.80%	60.10%	100%	100%	
PGV	0.1 m s^{-1}	3.70%	0	0	5.50%	0.50%	0.20%	0.20%	0	Assess using nonlinear analysis
	0.2 m s^{-1}	63.40%	5.30%	0.50%	26.50%	6.20%	3.10%	25.50%	1.10%	
	0.3 m s^{-1}	94.40%	33.60%	6.90%	47.70%	17.70%	10.70%	72.80%	16.60%	
	0.4 m s^{-1}	99.30%	66.40%	24.80%	63.60%	31.20%	21.20%	93.30%	48.10%	
	0.5 m s^{-1}	99.90%	86.00%	47.60%	74.60%	44.00%	32.50%	98.60%	74.80%	
	0.6 m s^{-1}	100%	94.70%	67.30%	82.00%	55.00%	43.10%	99.70%	89.50%	
PGD	0.1 m	42.30%	17.00%	8.10%	7.10%	1.10%	0.80%	27.30%	7.20%	Assess using nonlinear analysis
	0.2 m	72.60%	43.60%	27.40%	27.30%	8.40%	5.90%	61.60%	33.20%	
	0.3 m	85.70%	61.80%	44.60%	46.10%	19.80%	14.60%	79.40%	56.70%	
	0.4 m	91.90%	73.60%	57.70%	60.30%	31.80%	24.40%	88.40%	72.50%	
	0.5 m	95.10%	81.20%	67.40%	70.50%	42.80%	33.90%	93.10%	82.30%	
	0.6 m	96.90%	86.30%	74.50%	77.80%	52.30%	42.60%	95.70%	88.50%	

analysis of CFRDs, at least for this CFRD. However, the nonuniformity based on PGV and PGD was large. The correlation between the different IMs and DMs needs to be studied further in a future study.

This work was supported by the National Key Research and Development Program of China (Grant No. 2017YFC0404904) and the National Natural Science Foundation of China (Grant Nos. 51679029, 51508071 and 51779034).

1 Bayraktar A, Kartal M E. Linear and nonlinear response of concrete slab on CFR dam during earthquake. Soil Dyn Earthq Eng, 2010, 30: 990–1003
2 Zhou W, Hua J J, Chang X L, et al. Settlement analysis of the Shuibuya concrete-face rockfill dam. Comput Geotech, 2011, 38: 269–280
3 Xu B, Zou D G, Kong X J, et al. Dynamic damage evaluation on the slabs of the concrete faced rockfill dam with the plastic-damage model. Comput Geotech, 2015, 65: 258–265
4 Mojiri S, El-Dakhakhni W W, Tait M J. Shake table seismic performance assessment of lightly reinforced concrete block shear walls. J Struct Eng, 2015, 141: 04014105
5 Ellingwood B R, Tekie P B. Fragility analysis of concrete gravity dams. J Infrastruct Syst, 2001, 7: 41–48
6 Tekie P B, Ellingwood B R. Seismic fragility assessment of concrete gravity dams. Earthq Engng Struct Dyn, 2003, 32: 2221–2240
7 Lin L, Adams J. Lessons for the fragility of Canadian hydropower components under seismic loading. In: Proceedings of the 9th Canadian Conference on Earthquake Engineering. Ottawa, 2007. 1762–1771
8 Zhong H, Li H J, Bao Y L. Seismic risk analysis of an arch dam. Appl Mech Mater, 2013, 353-356: 2020–2023
9 Abdelhamid H, Mahmoud B, Hussein M. Seismic fragility and uncertainty analysis of concrete gravity dams under near-fault ground motions. Civil Environ Res, 2014, 5: 123–129
10 Kadkhodayan V, Aghajanzadeh M, Mirzabozorg H. Seismic assessment of arch dams using fragility curves. Civil Eng J, 2015, 1: 14–20
11 Morales-Torres A, Escuder-Bueno I, Altarejos-García L, et al. Building fragility curves of sliding failure of concrete gravity dams integrating natural and epistemic uncertainties. Eng Struct, 2016, 125: 227–235
12 Ghanaat Y, Patev R, Chudgar A. Seismic fragility analysis of concrete gravity dams. In: Proceedings of the 15th world conference on earthquake engineering, Lisbon, 2012
13 Hariri-Ardebili M A, Saouma V E. Probabilistic seismic demand model and optimal intensity measure for concrete dams. Struct Safety, 2016, 59: 67–85
14 Hariri-Ardebili M A, Saouma V E, Porter K A. Quantification of seismic potential failure modes in concrete dams. Earthq Engng Struct Dyn, 2016, 45: 979–997
15 Hariri-Ardebili M A, Saouma V E. Collapse fragility curves for concrete dams: Comprehensive study. J Struct Eng, 2016, 142:

04016075
16 Hariri-Ardebili M A, Saouma V E. Sensitivity and uncertainty quantification of the cohesive crack model. Eng Fract Mech, 2016, 155: 18–35
17 Ansari M I, Agarwal P. Categorization of damage index of concrete gravity dam for the health monitoring after earthquake. J Earthq Eng, 2016, 20: 1222–1238
18 Chen S S, Li G Y, Fu Z Z. Safety criteria and limit resistance capacity of high earth-rock dams subjected to earthquakes (in Chinese). Chin J Geotech Eng, 2013, 1: 59–65
19 Zhao J M, Liu X S, Yang Y S. Criteria for seismic safety evaluation and maximum aseismic capability of high concrete face rockfill dams (in Chinese). Chin J Geotech Eng, 2015, 12: 2254–2261
20 Ozkan M Y. A review of considerations on seismic safety of embankments and earth and rock-fill dams. Soil Dyn Earthq Eng, 1998, 17: 439–458
21 Zou D G, Xu B, Kong X J, et al. Numerical simulation of the seismic response of the Zipingpu concrete face rockfill dam during the Wenchuan earthquake based on a generalized plasticity model. Comput Geotech, 2013, 49: 111–122
22 Vamvatsikos D, Cornell C A. Incremental dynamic analysis. Earthq Engng Struct Dyn, 2002, 31: 491–514
23 Vamvatsikos D, Cornell C A. Applied incremental dynamic analysis. Earthq Spectra, 2004, 20: 523–553
24 Baker J W. Efficient analytical fragility function fitting using dynamic structural analysis. Earthq Spectra, 2015, 31: 579–599
25 Porter K, Kennedy R, Bachman R. Creating fragility functions for performance-based earthquake engineering. Earthq Spectra, 2007, 23: 471–489
26 Eads L, Miranda E, Krawinkler H, et al. An efficient method for estimating the collapse risk of structures in seismic regions. Earthq Engng Struct Dyn, 2013, 42: 25–41
27 Shome N. Probabilistic seismic demand analysis of nonlinear structures. Dissertation for Doctoral Degree. Providence: Stanford University, 1999
28 Newmark N M. Effects of earthquakes on dams and embankments. Géotechnique, 1965, 15: 139–160
29 Ling H I, Leshchinsky D, Mohri Y. Soil slopes under combined horizontal and vertical seismic accelerations. Earthq Engng Struct Dyn, 1997, 26: 1231–1241
30 Ghanaat Y. Failure modes approach to safety evaluation of dams. In: Proceedings of the 13th World Conference on Earthquake Engineering. Vancouver, 2004
31 Jia Y F, Xu B, Chi S C, et al. Research on the particle breakage of rockfill materials during triaxial tests. Int J Geomech, 2017, 17: 04017085
32 Xiao Y, Stuedlein A M, Chen Q, et al. Stress-strain-strength response and ductility of gravels improved by polyurethane foam adhesive. Int J Geomech, 2017
33 Xiao Y, Liu H L. Elastoplastic constitutive model for rockfill materials considering particle breakage. Int J Geomech, 2017, 17: 04016041
34 Xiao Y, Liu H L, Ding X, et al. Influence of particle breakage on critical state line of rockfill material. Int J Geomech, 2016, 16: 04015031
35 Liu J M, Liu H B, Zou D G, et al. Particle breakage and the critical state of sand: By Ghafghazi, M., Shuttle, D.A., DeJong, J.T., 2014. Soils and Foundations 54 (3), 451–461. Soils Found, 2014, 55: 220–222
36 Xiao Y, Sun Y F, Liu H L, et al. Model predictions for behaviors of sand-nonplastic-fines mixturesusing equivalent-skeleton void-ratio state index. Sci China Tech Sci, 2017, 60: 878–892
37 Liu J M, Zou D G, Kong X J, et al. Stress-dilatancy of Zipingpu gravel in triaxial compression tests. Sci China Tech Sci, 2016, 59: 214–224
38 Xiao Y, Sun Y F, Yin F, et al. Constitutive modeling for transparent granular soils. Int J Geomech, 2017, 17: 04016150
39 Duncan I M, Chang C Y. Nonlinear analysis of stress and strain in soils. J Soil Mech Found Division, 1970, 96: 1629–1653
40 Shen Z J, Xu G. Deformation behavior of rock materials under cyclic loading (in Chinese). Hydro-Science Eng, 1996, 2: 143–150
41 Hardin B O, Drnevich V P. Shear modulus and damping in soils: Design equations and curves. Geotech Spec Publ, 1972, 98: 667–692
42 Zou D G, Meng F W, Kong X J, et al. Residual deformation behavior of rock-fill materials (in Chinese). Chin J Geotech Eng, 2008, 30: 807–811
43 Ozkuzukiran S, Ozkan M Y, Ozyazicioglu M, et al. Settlement behaviour of a concrete faced rock-fill dam. Geotech Geol Eng, 2006, 24: 1665–1678
44 Yu X, Kong X J, Zou D G, et al. Linear elastic and plastic-damage analyses of a concrete cut-off wall constructed in deep overburden. Comput Geotech, 2015, 69: 462–473
45 Zou D, Zhou Y, Ling H L, et al. Dislocation of face-slabs of Zipingpu concrete face rockfill dam during Wenchuan earthquake. J Earthq Tsunami, 2012, 06: 1250007
46 Gooodman R E, Taylor R L, Brekke T L A. A model for the mechanics of jointed rock. J Soil Mech Found Div, 1968, 94: 637–659
47 Kong X J, Zhou Y, Zou D G, et al. Numerical analysis of dislocations of the face slabs of the Zipingpu concrete faced rockfill dam during the Wenchuan earthquake. Earthq Eng Eng Vib, 2011, 10: 581–589
48 Xu H, Zou D G, Kong X J, et al. Study on the effects of hydrodynamic pressure on the dynamic stresses in slabs of high CFRD based on the scaled boundary finite-element method. Soil Dyn Earthq Eng, 2016, 88: 223–236
49 Zou D G, Kong X J, Xu B. Geotechnical dynamic nonlinear analysis GEODYNA. Dalian: Dalian University of Technology, 2005
50 Westergaard H M. Water pressures on dams during earthquakes. Trans ASCE. 1933, 98: 418–432
51 Raphael J M. Tensile strength of concrete. J Am Concrete Inst, 1984, 81: 158–165
52 Liu J B, Lu Y D. A direct method for analysis of dynamic soil-structure interaction. Develop Geotech Eng, 1998, 83: 261–276
53 Swaisgood J R. Embankment dam deformations caused by earthquakes. In: Proceedings of the Pacific Conference on Earthquake Engineering. Christchurch, 2003
54 Darbre G R. Swiss guidelines for the earthquake safety of dams. In: Proceedings of the 13th World Conference on Earthquake Engineering. Vancouver, 2004
55 Tian J Y, Liu H L, Wu X Y. Evaluation perspectives and criteria of maximum aseismic capability for high earth-rock dam (in Chinese). J Disaster Prevent Mit Eng, 2013, 33(S1): 128–131